



Soft Matter

The dynamics of freestanding films: predictions for poly(2-chlorostyrene) based on bulk pressure dependence and thoughtful sample averaging

Journal:	<i>Soft Matter</i>
Manuscript ID	SM-ART-08-2021-001175.R1
Article Type:	Paper
Date Submitted by the Author:	27-Sep-2021
Complete List of Authors:	White, Ronald; Dartmouth College, Chemistry Lipson, Jane; Dartmouth College, Chemistry

SCHOLARONE™
Manuscripts

The dynamics of freestanding films: predictions for poly(2-chlorostyrene) based on bulk pressure dependence and thoughtful sample averaging

Ronald P. White and Jane E.G. Lipson*

Department of Chemistry,
Dartmouth College, Hanover, NH 03755

Abstract:

In this paper we model the segmental relaxation in poly (2-chlorostyrene) 18 nm freestanding films, using only data on bulk samples to characterize the system, and predict film relaxation times (τ) as a function of temperature that are in semi-quantitative agreement with film data. The ability to translate bulk characterization into film predictions is a direct result of our previous work connecting the effects of free surfaces in films with those of changing pressure in the bulk. Our approach combines the Locally Correlated Lattice (LCL) equation of state for prediction of free volume values (V_{free}) at any given density (ρ), which are then used in the Cooperative Free Volume (CFV) rate model to predict $\tau(T, V_{\text{free}})$. A key feature of this work is that we calculate the locally averaged density profile as a function of distance from the surface, $\rho_{\text{av}}(z)$, using the CFV-predicted lengthscale, $L_{\text{coop}}(z)$, over which rearranging molecular segments cooperate. As we have shown in the past, $\rho_{\text{av}}(z)$ is significantly broader than the localized profile, $\rho(z)$, which translates into a relaxation profile, $\tau(z)$, exhibiting a breadth that mirrors experimental and simulated results. In addition, we discuss the importance of averaging the log of position dependent relaxation times across a film sample ($\langle \log \tau(z) \rangle$), as opposed to averaging the relaxation times, themselves, in order to best approximate a whole sample-averaged value that can be directly compared to experiment.

Corresponding Author

*E-mail: jane.lipson@dartmouth.edu

1 Introduction

The study of dynamic properties of polymer melts and other molecular liquids (relaxation times, viscosity, diffusion, etc.) as they approach their glass transition has attracted longstanding research interest.^{1–10} Experiments which test the effects on system dynamics from changing the pressure, in addition to changing temperature, have yielded fundamental insight,^{1,2} leading to a more complete understanding of how structural relaxation times, $\alpha(T,V)$, depend on underlying independent contributions from both temperature (T) and volume (V). There has been significant recent interest in the effects induced by the presence of interfaces, often called the nanoconfinement effect,^{10–21} which can lead to information about the length scale associated with mechanisms of dynamic relaxation. In recent work we^{22–25} and others^{26–32} have explained some of the important connections between the influence of interfaces and effects from changing pressure (changing density).

Here we investigate the pressure dependent and interfacial dynamics, of poly(2-chlorostyrene) (P2ClS) using the Cooperative Free Volume (CFV) rate model.^{33,34} The model accounts for independent contributions from temperature and density (i.e. $\alpha(T,V)$), allowing us to explicitly incorporate the effects from interfacial density changes. Our analysis begins with predictions for free volume, a natural variable for analyzing relaxation results, via analysis of bulk PVT data using the Locally Correlated Lattice (LCL) equation of state.^{35,36} We then apply the CFV model to the experimental α -relaxation times of bulk P2ClS from dielectric spectroscopy, illustrating that the form predicted by CFV, $\tau \propto \exp[f(T) \times (1/V_{\text{free}})]$ is well obeyed. This CFV analysis of bulk P2ClS provides characteristic information that is then used (along with density profiles based on PVT and surface tension data) to predict how relaxation times change on the

nanometer scale across a P2CIS free surface. We then combine our understanding of bulk behavior and predictions for free surface effects to form an independent prediction for the *overall* relaxation time of P2CIS freestanding films as a function of temperature. Finally, we test our model predictions with existing experimental film data and find very good agreement.

Alongside the CFV approach, there are a number of other models for the dynamics of confined systems; examples can be found in the articles and reviews in references ^{10,15,16,28,29,37–41}. In some cases^{28,29} (similar to our work here) strong connections are made with bulk pressure dependent dynamics, a particular example being the density scaling approach.^{1,2,8,42–45} Other models build on different connections, e.g. detailed pair correlations,⁴⁰ percolation and heterogeneous dynamics,^{37,38,41} and string models.³⁹ Recently in reference ²⁵, we briefly surveyed some of these approaches to place the CFV model in context.

2 Interfacial dynamics and bulk pressure dependent dynamics

Interfacial systems are inhomogeneous since they involve a free surface and a local density that changes from bulk-like to zero. However, we have found that^{22–25} the changes in dynamics induced by the interface are strongly analogous to those arising from a pressure-induced density change in the homogeneous bulk. Experimental data for a bulk system's temperature and volume dependent relaxation behavior show that segmental relaxation times follow a general pattern,

$$\tau(T, V) \propto \exp[f(T) \times g(V)]. \quad (1)$$

The evident *multiplicative* coupling of $f(T)$ and $g(V)$ has consequences that underlie many important trends, and these patterns appear whether the material is in bulk form or in thin films. For thin films the density change at the interface will affect the value of the density dependent $g(V)$

function, while of course in the bulk this term is sensitive to changing pressure. In both cases the effect becomes more pronounced with decreasing T because lower temperatures increase the value of $f(T)$, the factor which multiplies the changing $g(V)$ function.²²

Eqn (1) will be the starting point in building our model for interfaces; what makes this possible is the transferability of $f(T)$. The fact that eqn (1) describes pressure dependent bulk dynamics obviously means that the same function, $f(T)$, applies at any choice of volume (pressure). We find that the same $f(T)$ also applies (at least approximately) when the material is in film form. Strong evidence for this is as follows.

Starting from eqn (1) a general power law form can be derived, $\tau_2(T) \propto \tau_1(T)^c$, which connects the relaxation behavior of two isobars, "1" and "2"; the exponent $c = g(V_2(T))/g(V_1(T)) = V_{\text{free1}}(T)/V_{\text{free2}}(T)$ (V_{free} defined below) depends only on the two density contributions and is an approximate constant.²² Linear power law plots of $\log \tau_2(T)$ vs. $\log \tau_1(T)$ show that this form is indeed followed for any two isobars of the bulk material, e.g. high P and low P . Importantly, this very same power law form also applies when comparing polymer film relaxation data with that of bulk (both at the same pressure), an observation first reported in Diaz-Vela et al.⁴⁶ Because the power law relationship can only be derived when there is a common $f(T)$ function, we must have $f_1(T) = f_2(T) = f(T)$ even when "1" and/or "2" is a film. In our approach, we will determine the characteristic $f(T)$ contribution for P2CIS by modeling its bulk behavior, and then apply this same function to P2CIS films. This will be fully described further below after introducing the CFV model which is our route to expressing $f(T)$ and $g(V)$ analytically.

In the case of interfaces the effective density needed as input for $g(V)$ will depend upon the distance from the interface; that is, we will treat $g(V)$ here as a position (z) dependent function. (Note alternatively, if dealing with a whole film sample, one can assign an overall $g(V)$ that will change with film thickness (h), due to the changing relative contribution from the lower density interfacial region.) Segments near a free surface have fewer surrounding neighbors, analogous to what happens when lowering the density in a homogeneous bulk environment. However, a key question is: which segments count as neighbors? To what distance out from a given point does the influence of the other segments extend? The answer reflects the mechanistic cooperativity that is an integral feature of local segmental relaxation.

We define L_{coop} to be the distance that spans a group of cooperating segments. Note that because L_{coop} is based on *intermolecular* encounters, it must clearly be larger than a molecular segment e.g. 2 or 3 coordination shells. This makes L_{coop} wider than the gradient in a typical local density profile ($\rho(z)$), which means that the density input for $g(V)$ at a given position, z , cannot simply be the value of $\rho(z)$, unless z is located well within the bulk interior. Furthermore, we expect the number of segments that cooperate, and thus L_{coop} , to be a changing function of the density and thus position, i.e. $L_{\text{coop}}(z)$. The CFV model predicts this crucial dependence based on the condition that the cooperative region, $V_{\text{coop}}(z)$, must contain the same characteristic critical free volume, v^* necessary for a segment to move a distance on the order of its own size (e.g. necessary for local relaxation).

The appropriate input for the $g(V)$ function at any given position, z , will be the locally *averaged* density, $\rho_{\text{av}}(z)$, which is the average taken inside the region containing the cooperating segments centered around z . We calculate $\rho_{\text{av}}(z)$, based on the local density, $\rho(z)$, as follows

$$\rho_{\text{av}}(z) = \frac{1}{V_{\text{coop}}(z)} \int \rho(z') dx' dy' dz' \quad (2)$$

$\rho(z)$ and $\rho_{\text{av}}(z)$ depend only on z , the position in the direction normal to the interface. The integration (average) is carried out over the values of x', y', z' that are within a cooperative region having a volume, $V_{\text{coop}}(z)$, that surrounds a point, x, y, z . The size of the region, $V_{\text{coop}}(z)$, is such that it contains the above noted characteristic critical free volume, v^* . Given a local density profile of the material's free surface (details below), we can therefore solve for $\rho_{\text{av}}(z)$ and $V_{\text{coop}}(z)$ (thus $L_{\text{coop}}(z)$) self consistently, based on the constancy of v^* . We obtain the value of v^* by knowing the value of L_{coop} in the bulk at just a single reference temperature. We have a sensible way to estimate this within say, about $\pm 25\%$ (details below); the model will then predict all the changing values of $L_{\text{coop}}(z)$ across the interface and at any other temperature.

3 The CFV model and application to bulk P2CIS

A key feature of the cooperative free volume (CFV) rate model^{33,34,47} is that it expresses $g(V)$ in terms of the free volume, V_{free} , as predicted by analysis of thermodynamic data. Obtained in that way, V_{free} turns out to be a natural variable for this purpose; it allows for the same mathematical form ($g(V) \propto 1/V_{\text{free}}$) to be used for all systems.

Here we highlight this point, that the V_{free} values used in CFV are based on independent thermodynamic analysis, because other models use *a posteriori* fitting of dynamics data to extract

an estimate of V_{free} , a practice that undermines its physical meaning. In our definition V_{free} is given by

$$V_{\text{free}} = V - V_{\text{hc}} \quad (3)$$

where V is the system's total volume and V_{hc} is its characteristic limiting hard-core volume at close packing. V_{hc} is a material-dependent constant, independent of temperature and pressure. We apply the locally correlated lattice (LCL) equation of state (EOS)^{35,36} to analyze a system's pressure, volume, temperature (PVT) data in order to determine the set of LCL molecular parameters (specific to each material) that leads to V_{hc} , and thus the system's V_{free} values at any given T, P . (For the interested reader, another very simple route to V_{hc} and V_{free} based on PVT data has been described and tested in another recent paper.⁴⁷) Applying LCL to P2CIS PVT data⁴⁸ we find $V_{\text{hc}} = 0.733$ mL/g. More details on the LCL analysis of P2CIS are provided in the Electronic supplementary information (ESI).

In the CFV model the relaxation mechanism is both thermally activated and cooperative. This is analogous to the model of Adam and Gibbs,⁴⁹ however, in CFV the cooperativity is dictated by free volume rather than configurational entropy. The relaxation process requires the rearrangement of a cooperating group consisting of n^* segments, where each segment is capable of donating an amount of free volume equal to V_{free}/N (where N is the total number of segments in the system). For each segment there will be an energetic cost of Δa in order for it to move. Therefore the total activation energy for the rearrangement is $E_{\text{act}} = n^* \Delta a$. To determine how n^* depends, functionally, on V_{free} we expect (assume) that it is necessary for the group, overall, to gather a critical amount of free volume, v^* ; this should be a characteristic constant of the material, i.e. enough space to allow the entry or full passage of another segment. Dividing v^* by the free

volume that a single segment can donate therefore gives $n^* = v^*/(V_{\text{free}}/N)$, and this leads to the key relation, $E_{\text{act}} \propto n^* \propto 1/V_{\text{free}}$. As noted above, the concept of accruing a constant critical free volume (v^*) is important here in dictating how the cooperative distance, $L_{\text{coop}}(z)$, and thus ultimately the local activation energy, changes with position near the interface.

The Boltzmann factor for the relaxation rate is $\exp[-E_{\text{act}}/T] \propto 1/\tau$, and we can now substitute $E_{\text{act}} = n^*\Delta a$ and $n^* \propto 1/V_{\text{free}}$ to give the general CFV form for relaxation times,

$$\tau = \tau_{\text{ref}} \exp\left[n^* \times \left(\frac{\Delta a(T)}{T}\right)\right] = \tau_{\text{ref}} \exp\left[\left(\frac{1}{V_{\text{free}}}\right) \times f(T)\right] \quad (4)$$

The multiplicative coupling of T, V contributions in eqn (4) shows how CFV predicts and explains the fundamental form of eqn (1), viz. $\tau(T, V) \propto \exp[g(V) \times f(T)]$. We identify $g(V) \propto 1/V_{\text{free}}$, and $f(T) \propto \Delta a(T)/T$.

Our tests of the CFV model against experimental data have shown that the basic form predicted by eqn (4) holds across a wide range of polymer melts and small molecule glassforming liquids,^{34,47,50,51} as well as for simulated systems.^{33,52} Written equivalently as $\ln(\tau/\tau_{\text{ref}}) \propto (1/V_{\text{free}}) \times (\Delta a(T)/T)$, this form predicts that on isotherms the log of segmental relaxation times will be linearly proportional to inverse free volume, and that the slope of each linear isotherm will depend on its temperature. Further, by the simplest possible assumption of a constant Δa (more below), the slopes are predicted to increase with decreasing T . This is indeed the pattern followed by the P2ClS melt. Fig. 1a shows the P2ClS T, P -dependent α -relaxation times measured via dielectric spectroscopy⁵³; the $\log \tau$ vs. $1/V_{\text{free}}$ isotherms are linear and the slopes increase with decreasing T . Note that the values plotted on the ordinate represent experimental results from

dielectric relaxation experiments, while those on the abscissa are from thermodynamic PVT analyses; they have been determined independently, and therefore support our conclusion that there is a strong connection between V_{free} and dynamic relaxation.

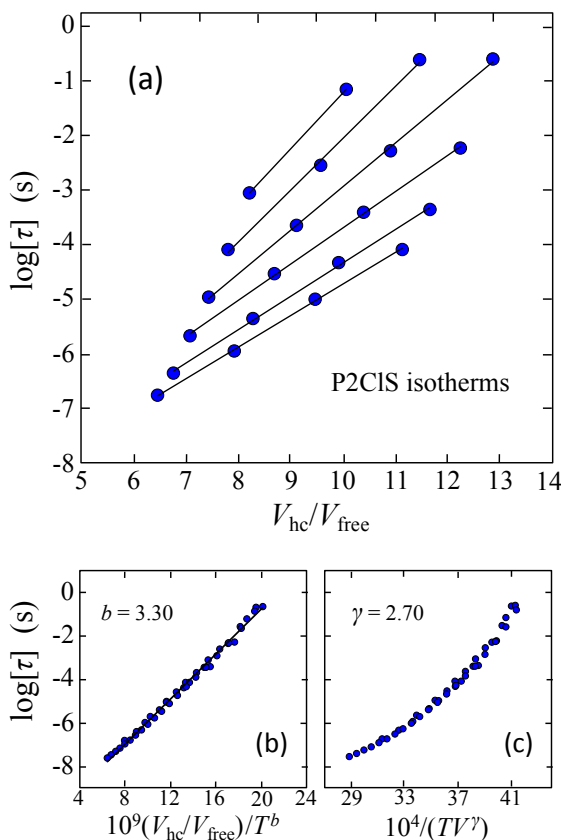


Fig. 1 P2CIS bulk pressure dependent dynamics. Panel (a): α -relaxation times on isotherms, plotted as $\log \tau$ vs. inverse relative free volume ($V_{\text{hc}}/V_{\text{free}}$). The isotherms are linear with T -dependent slopes, as predicted by the CFV model. From top to bottom, $T = 442, 454, 466, 478, 490, 502$ K; experimental data⁵³ are shown as points, and the lines are the corresponding linear fits. Panel (b) shows the data collapsed into a single line according to CFV eqn (5) giving a b parameter value of 3.3. Panel (c) shows the data collapsed using the density scaling approach giving a γ parameter value of 2.7.

We now turn to the details for the functional temperature dependence, $f(T)$. We have found the simplifying assumption of constant Δa works well at high T , e.g. for describing $\alpha(T, V)$ in the Arrhenius-nonArrhenius crossover regime. However, in order to accurately capture the

experimental data as it extends into lower T , we must treat $\Delta a(T)$ as function of T (although it remains independent of volume). In practice, we apply a simple empirical T -dependent form, $f(T) \sim \Delta a(T)/T \sim 1/T^b$. Here the material specific scaling exponent b is roughly analogous to the scaling of V in density scaling approaches.^{1,2,8,42-45} This leads to the following working expression

$$\ln \tau = \left(\frac{V_{\text{hc}}}{V_{\text{free}}} \right) \left(\frac{T^*}{T} \right)^b + \ln \tau_{\text{ref}} \quad (5)$$

The material specific parameters, $b, T^*, \tau_{\text{ref}}$, are determined from bulk system dynamics data; alternatively b can also be determined using $T_g(P)$ from PVT data.

The form of eqn (5) indicates that with the proper choice of b , a plot of $\log \tau$ vs. $1/(V_{\text{free}} T^b)$ will collapse all the T, P -dependent data in Fig. 1a into a single line. This is shown in Fig. 1b where simple trial and error adjustment indicates a P2CIS b value of about 3.3. For comparison, a density scaling analysis is shown in Fig. 1c where the plot of $\log \tau$ vs. $1/(TV^\gamma)$ collapses into a single curve with $\gamma = 2.7$.

To complete the characterization of eqn (5) for P2CIS, the remaining parameters, T^* and τ_{ref} , will follow from the slope and intercept of the line in Fig. 1b. Alternatively, all three parameters ($b, T^*, \tau_{\text{ref}}$) can be found by simultaneous least squares fitting, which leads to essentially equivalent results. The full set of P2CIS parameters is: $b = 3.30$, $T^* = 568.1$ K, $\log \tau_{\text{ref}} (\text{/s}) = -11.36$, (or equivalently, $\ln \tau_{\text{ref}} = -26.17$); note we apply eqn (5) as written using natural logarithms (\ln), and then convert the results to base 10 logarithms (\log) when plotting results to match standard experimental representations. With bulk P2CIS fully characterized we now show the resulting CFV model curves (eqn (5)) along with the corresponding experimental data plotted in the form

of $\log \tau$ vs. $1/T$ isobars in Fig. 2. (From bottom to top, isobars correspond to $P = 1$ atm, 50MPa, 100MPa, 150MPa, 200MPa.)

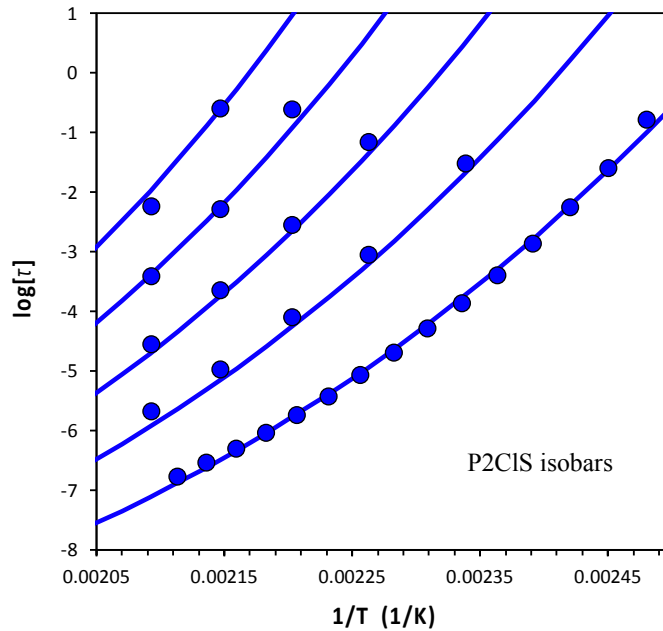


Fig. 2 P2CIS bulk pressure dependent dynamics: α -relaxation times on isobars. CFV model results shown as curves, and experimental data⁵³ shown as points. From bottom to top, $P = 1$ atm, 50 MPa, 100 MPa, 150 MPa, and 200 MPa.

4 P2CIS interfacial dynamics and freestanding films

We will now extend the use of the CFV eqn (5) to capture P2CIS relaxation times as a function of temperature and density from the case of the bulk to interfaces, as relaxation data for these systems show analogous change with temperature and, in this scenario, position dependent locally averaged density, $\rho_{av}(z)$. We therefore apply the same $f(T) = (T^*/T)^b$ function to the P2CIS interface as we found for bulk (same τ_{ref} as well). Furthermore, the $g(V) = V_{hc}/V_{free}$ function

remains based on the same bulk P2CIS PVT analysis, although it will now manifest in eqn (5) as a position dependent quantity. This will appear as $(V_{\text{hc}}/V_{\text{free}})(z)$, which follows from the locally averaged density, $\rho_{\text{av}}(z)$ (eqn (2) above), according to $(V_{\text{free}}/V_{\text{hc}})(z) = (\rho_{\text{hc}}/\rho_{\text{av}}(z)) - 1$, where $1/\rho_{\text{hc}}$ = close-packed volume V_{hc} per mass.

In order to obtain $\rho_{\text{av}}(z)$ we need the local density profile, $\rho(z)$. We calculate $\rho(z)$ based on bulk PVT and surface tension data. Specifically, we use the LCL EOS (which as noted above was fit to the P2CIS PVT data⁴⁸) combined with the square gradient approximation^{54–56} where the gradient parameter is fit to the P2CIS surface tension.^{57,58} Details on these calculations are provided in the ESI. The resulting P2CIS free surface local density profile, $\rho(z)$, at $T = 425\text{K}$ is shown in Fig. 3a (the blue curve). The gradient in $\rho(z)$ is fairly narrow, going from bulk-like density to zero over a region that is only about 1 nm wide (less than a Kuhn length). This is similar to what we found for PS²⁵ and is consistent with calculations on other polymers⁵⁶ and results from simulations.^{59–63}

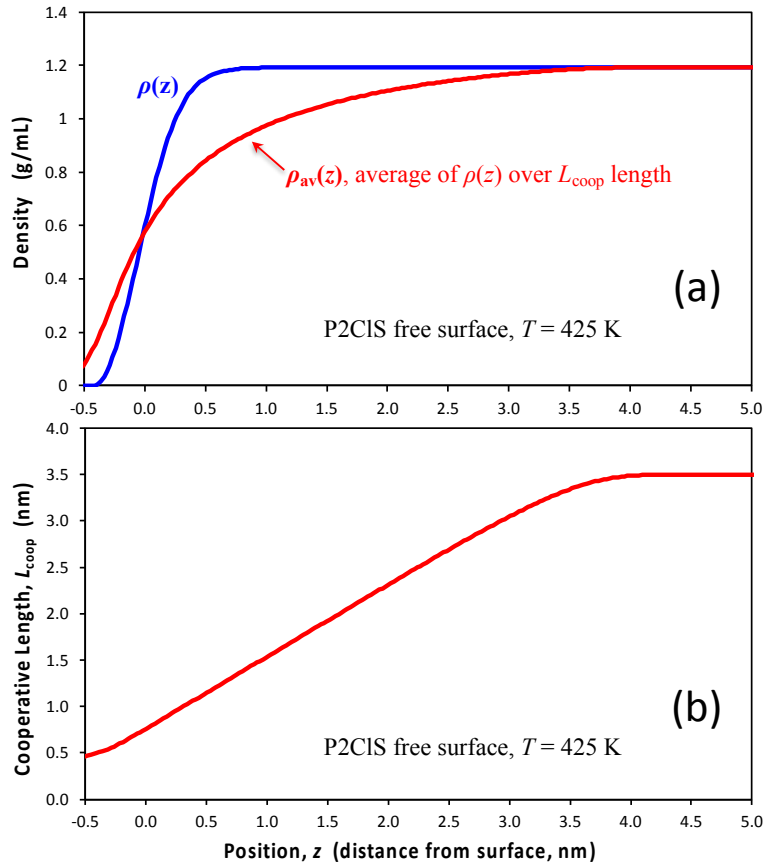


Fig 3 Local density, $\rho(z)$, locally-averaged density, $\rho_{av}(z)$, and cooperative length, $L_{coop}(z)$, as a function of position, z , across a P2CIS free surface at $T = 425$ K, $P = 1$ atm. Panel (a) shows $\rho(z)$ (blue curve) and $\rho_{av}(z)$ (red curve), and panel (b) shows $L_{coop}(z)$. $\rho(z)$ is calculated using the LCL EOS model based on PVT data and surface tension data, and $\rho_{av}(z)$ and $L_{coop}(z)$ then follow from this result based on eqn (2) and the requirement that the cooperative region must enclose the characteristic critical free volume, v^* (see text).

As noted above, solving for $\rho_{av}(z)$ in eqn (2) requires knowing v^* for the material of interest, and then assuming it to be constant. We first identify the value of L_{coop} , the cooperative lengthscale, in the bulk at a single reference temperature, denoted $L_{coop:ref}$, and then find v^* as the *free* volume inside the volume, $(2L_{coop:ref})^3$. At the reference state this is the volume that contains the essential available free volume required for a segmental relaxation to occur. We will use the same approximate value for $L_{coop:ref}$ that we used in our previous work²⁵ for PS (3.5 nm) because the PS and P2CIS Kuhn lengths are expected to be similar (about 1.5 nm⁶⁴), and we set this at a

central reference temperature of 425 K ($P = 1$ atm) which is about 25 degrees above the P2CIS T_g . $L_{\text{coop:ref}} = 3.5$ nm corresponds to about 2.3 Kuhn lengths, implying a cooperating distance covering about 2 or so coordination shells. As described in our previous work²⁵ this approximation for $L_{\text{coop:ref}}$ was also based on the point where our simple 2-layer CFV model interprets the bulk-like layer to disappear when applied to Al-capped P4CIS films of decreasing thickness. We expect this approximation for the bulk $L_{\text{coop:ref}}$ to be reasonable within about $\pm 25\%$. Indeed, we show here that it leads to semi-quantitative predictions. If closer agreement is desired, it could be treated as a fitting parameter (i.e. it could be fit to the P2CIS freestanding film data⁶⁵).

With the single value now set for the bulk $L_{\text{coop:ref}}$, which also sets v^* , we can now predict how $L_{\text{coop}}(z)$ changes with position across the interface at any temperature. Since the required cooperating region must always contain the same amount of free volume we expect that $L_{\text{coop}}(z)$ will decrease on moving toward the free surface. Solving eqn (2) self consistently with the condition that $V_{\text{coop}}(z)$ contains a free volume of $[1 - (\rho_{\text{av}}(z)/\rho_{\text{hc}})]V_{\text{coop}}(z) = v^*$, yields both $\rho_{\text{av}}(z)$ and $L_{\text{coop}}(z)$ ($V_{\text{coop}}(z)$). (See our previous work for more details.²⁵) The result for $L_{\text{coop}}(z)$ is shown in Fig. 3b (corresponding to the P2CIS free surface at $T = 425$ K, $P = 1$ atm). About 1 nm from the interface $L_{\text{coop}}(z)$ is about 1.5 nm (roughly one Kuhn length). By 4 nm or more from the interface, $L_{\text{coop}}(z)$ has achieved its bulk value of 3.5 nm (2.3 Kuhn lengths),

The corresponding self consistent result for $\rho_{\text{av}}(z)$ is shown by the red curve in Fig. 3a ($T = 425$ K, $P = 1$ atm). In contrast to the *local* density $\rho(z)$, $\rho_{\text{av}}(z)$ deviates from the bulk value deeper into the interior because it reflects an averaged environment over an *intermolecular* length scale (e.g. $\sim 1, 2, 3$ Kuhn lengths). Of course the shape of $\rho_{\text{av}}(z)$ also differs from the shape of $\rho(z)$

because the cooperative lengthscale to which $\rho_{\text{av}}(z)$ is coupled depends, itself, on z . Results for $\rho_{\text{av}}(z)$ calculated at other temperatures (used below for $\tau(T, z)$) are similar to what is shown here at $T = 425$ K, but will reflect small changes in $\rho(z)$ and on the bulk L_{coop} value at that temperature.

The reasoning above explains why a single value of $\rho(z)$ at z cannot capture the degree intermolecular crowding at positions near the interface; its gradient is so steep in that region that the value of $\rho(z)$ could be bulk-like at one position, and at just a single near neighbor distance away its value could be closer to half of that. Because $\rho_{\text{av}}(z)$ accounts for the surrounding intermolecular environment, it correlates strongly with local relaxation dynamics. Local averaging is unnecessary within a bulk sample, where the density is homogeneous, but becomes important near interfaces.

Turning to relaxation times, we take the result for $\rho_{\text{av}}(z)$ (Fig. 3a) and compute the relative free volume as a function of position, $(V_{\text{free}}/V_{\text{hc}})(z) = (\rho_{\text{hc}}/\rho_{\text{av}}(z)) - 1$, and this result is input into eqn (5) to obtain $\tau(z)$ using the same parameters that describe the P2CIS bulk dynamics (Fig. 2). Examples of resulting relaxation profiles at three different temperatures are shown in Fig. 4. Here, rather than just the ~ 5 nm span shown in Fig. 3, the relaxation profiles cover an entire 18 nm freestanding P2CIS film, which has two free surfaces and a bulk-like plateau region in between. The temperature values for the $\tau(z)$ profiles correspond to $T = 410, 425, 440$ K; note in all cases, our results for films and/or interfaces correspond to ambient pressure conditions, $P = 1$ atm.

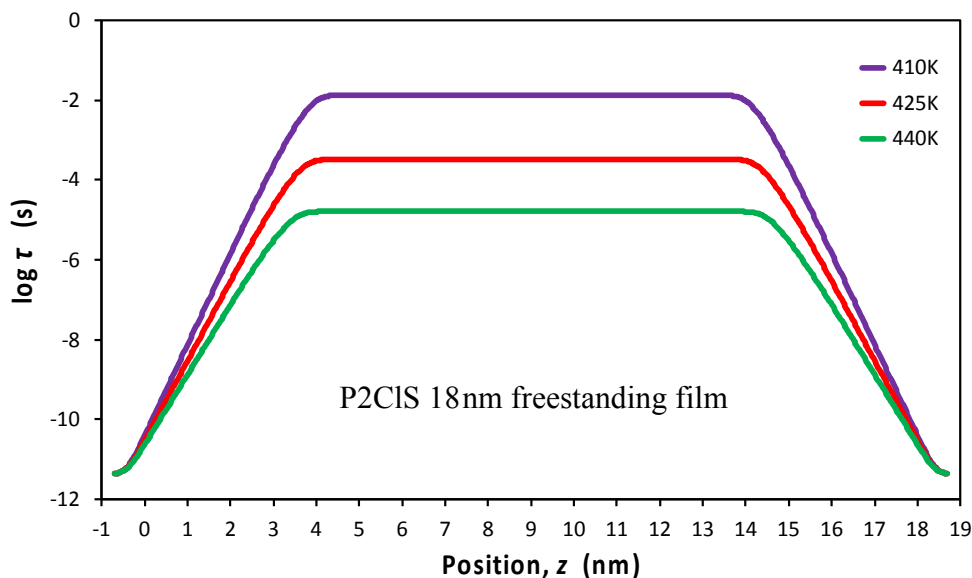


Fig. 4 18 nm freestanding P2CIS film: CFV predicted relaxation times, $\tau(z)$, as a function of position at three different temperatures, $T = 410, 425,$ and 440 K. $\tau(z)$ at any given T is based on inputting the position dependent $(V_{\text{free}}/V_{\text{hc}})(z) = (\rho_{\text{hc}}/\rho_{\text{av}}(z)) - 1$ into Eqn (5) with parameters, $b, T^*, \tau_{\text{ref}}$, determined from P2CIS bulk dynamics.

The CFV model profiles in Fig. 4 show that near the interfacial region $\tau(z)$ deviates from the bulk value over a span of more than 4 nm, with a broad shape that is significantly extended relative to the gradients in the corresponding local density profiles $\rho(z)$ (~ 1 nm wide); this is consistent with results from simulation.^{14,59–63,66}

Comparison of the $\tau(z)$ profiles at different temperatures shows that the plateau height (the bulk relaxation time) increases with decreasing T as expected. Also, the location of the plateau shifts further into the interior (i.e. the relaxation gradient gets wider) as T decreases, and this is also consistent with trends observed in simulations. This is a consequence of how the bulk L_{coop} is increasing (due to increasing ambient density) as T decreases,²⁵ which means that there is an increased distance over which a deviation in $\rho(z)$ will contribute, as part of the cooperative region.

The result is that $\rho_{av}(z)$ and $\tau(z)$ deviate from their respective bulk values over larger distances from the interface.

We now consider the *overall* relaxation time, characteristic of the entire freestanding P2CIS film sample. Here we will compare with existing experimental data on 18 nm "stacked" freestanding films studied via dielectric spectroscopy in Fukao et al.⁶⁵ where relaxation times were reported over a range of temperature. (Some examples of calorimetric studies on stacked films are in Koh et al.^{67,68}) Experimentally, the procedure for the Fukao et al. dielectric measurements involved the samples to be capped with Aluminum (Al); in the case of the multiple 18 nm stacked films only the two outermost films would have one of their interfaces supported (capped) by an Al substrate surface. Therefore, most of the interfaces contributing to the dynamics in the overall sample are "free", in the sense that they are not joined to each other or to a substrate. We therefore consider each film as corresponding to an idealized freestanding film. A focus in the Fukao et al.⁶⁵ paper was to study the change in the relaxation rate as the sample gradually transformed upon annealing, that is, as the thin films merged into a bulk-like thicker film. Our particular interest here is in the data that were reported at zero annealing time, i.e. before the stacked films were annealed into a more bulk-like sample. The data for these 18 nm stacked films were taken from figure 9 of that work. We also used data for the bulk sample, i.e. for the thicker 120 nm film (which had equivalent dynamics to that of the stacked sample once it had undergone a very long annealing time).

Fig. 5 shows a comparison of the Fukao et al.⁶⁵ data plotted together ($\log \tau$ vs. $1/T$) with the Schwartz et al.⁵³ P2CIS bulk data, the latter of which was used to parameterize the CFV model.

Note that the 120 nm film data, which is what effectively counts as the bulk P2CIS data from Fukao et al. (open black symbols), lie slightly above the corresponding ambient pressure ($P = 1$ atm) bulk data from Schwartz et al (solid blue symbols). These small differences between results from different laboratories are common, for example, often being caused by a difference in the polymer sample. Therefore, in order to properly represent the change in the 18 nm film dynamics relative to a strictly analogous bulk sample, the bulk data from the two labs should be aligned. We apply a shift of $\log \tau = -0.4$ to the 120 nm bulk-like film data from Fukao et al to line it up with the Schwartz et al P2CIS results; this same shift must then also be applied to the 18 nm film data. The results are shown by the open red and solid red symbols respectively; this is equivalent to a simple shift of the VFT curve by an additive constant.

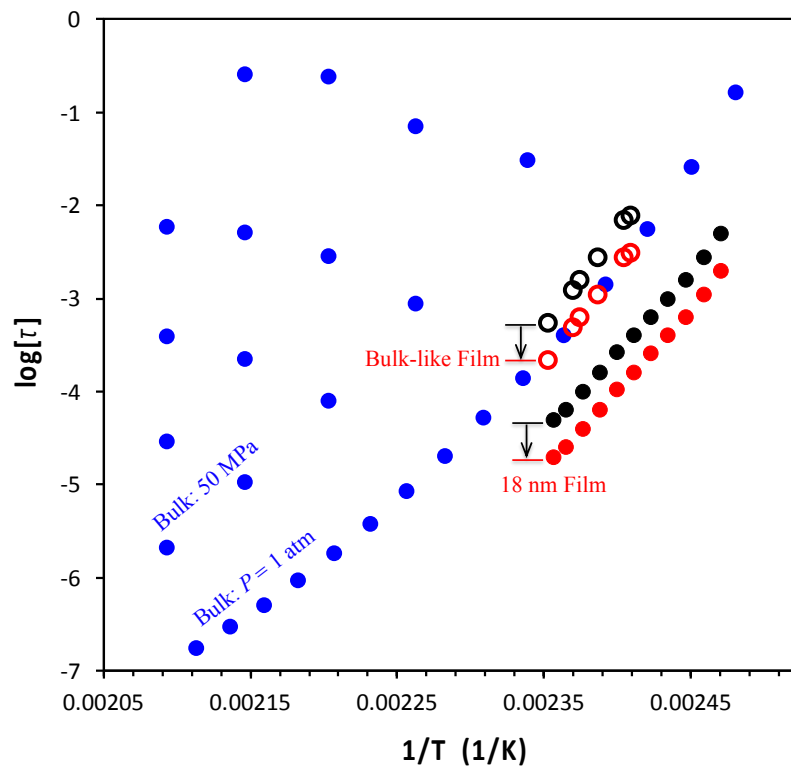


Fig. 5 P2CIS relaxation times as a function of inverse temperature: comparison of experimental data for films and bulk. Solid blue symbols correspond to bulk data from Schwartz et al.⁵³; these data include results for the standard isobar at ambient pressure (marked in the figure) as well as isobars at higher pressure. (The

same bulk data is also shown in Fig. 2). The experimental data for the 18 nm film and the bulk-like 120 nm film (ambient pressure) are from Fukao et al.⁶⁵ and are shown by the solid black symbols and open black symbols respectively. These data were aligned with the Schartz et al data by shifting the ordinate values of both sets down by 0.40 (solid red and open red symbols); this shift brings the bulk-like 120 nm film into overlap with the corresponding ambient bulk data of Schwartz et al. while preserving the difference between the bulk and the 18 nm film. See main text for details.

We now turn to the question of how to properly calculate the model prediction for the overall relaxation time for a whole film sample based on the model relaxation profile (Fig. 4). We begin by emphasizing that it would not be correct to define the film-averaged relaxation time by simply taking a mass weighted average of the τ value at each point in the film. That is,

$$\tau_{\text{film}} \neq [\int \rho(z) dz]^{-1} \int \tau(z) \rho(z) dz. \quad (6)$$

(Integrations extend over the whole film, and $\int \rho(z) dz$ is the film's mass per area.) The integration described by eqn (6) treats the sample τ_{film} , mathematically, as a "mean value" of τ . However, in the context of most studies, the intended physical meaning of τ is much closer in spirit to either a "median value", e.g. the time when half (or some other specified fraction) of a population has relaxed, or, in the case of standard dielectric spectroscopy analyses, a "most probable value". The latter follows because $\tau (= 1/2\pi f_{\text{max}})$ is associated with the peak frequency (f_{max}) of the dielectric loss curve, $\varepsilon''(f)$ vs. $\log f$, where the area under this curve is proportional to the number density of participating dipoles (i.e. proportional to the dielectric strength, $\Delta\varepsilon$).⁶⁹ The distinction between "mean", "median", and "most probable", can be significant in glassy dynamics where the relaxation function for the population is typically spread out in time over several orders of magnitude.

To illustrate this point, consider that applying eqn (6) to the $\tau(z)$ profile for the 18 nm film at $T = 425\text{K}$ gives $\log \tau_{\text{film}} = -3.63$ (τ in units s). This treatment yields a shift of $\Delta \log \tau = -0.15$ relative to the corresponding bulk value ($\log \tau = -3.48$). Referring back to the actual plot of the underlying $\tau(z)$ profile in Fig. 4, this suggests that the one third of the sample in the interfacial region has had very little impact in the film sample average. Since using eqn (6) leads to the "mean value" of τ , as opposed to $\log \tau$, important contributions covering several orders of magnitude will not be distinctly considered, but instead all weighted effectively as if they were $\tau = \text{zero}$ compared to the larger (bulk-like) relaxation times, an effect that will skew the results. In other words, taking the log of this mean τ will produce a result that will always be heavily weighted toward (the log of) the largest relaxation times.

To obtain τ for a whole sample, ideally one should consider that in an experimental sample there is an entire spectrum of values associated with each position, z . Adding these at each position (i.e. adding together each position dependent "sub-spectrum") would give an overall sample spectrum from which a peak value for the entire sample could be obtained. Our model (at any given location, whether interfacial or bulk) does not provide a whole spectrum, of course, so we must work with just the single τ value corresponding to the peak in the standard dielectric ε'' vs. $\log f$ spectrum. In particular we imagine that $\tau(z)$ at each position, z , will identify the peak location for each contributing sub-spectrum that would be hypothetically measured at each z .

Given that the area under a curve of ε'' vs. $\log f$ (not ε'' vs. f) is proportional to the number density of participating dipoles (i.e. $\Delta \varepsilon \propto \int \varepsilon''(f) \ln f$), and assuming that for each region in the sample (each position, z) the distribution is not too strongly skewed (asymmetric) about its peak

value, then taking the mean of $\log \tau$ should provide a reasonable approximation to the location of the peak in the overall ϵ'' vs. $\log f$ dielectric spectrum for the whole sample (i.e. $-\log[2\pi f_{\max}]$). That is, we will approximate τ_{film} according to

$$\log \tau_{\text{film}} \approx \left[\int \rho(z) dz \right]^{-1} \int \log \tau(z) \rho(z) dz \quad (7)$$

or equivalently, $\tau_{\text{film}} \approx \exp \left\{ \left[\int \rho(z) dz \right]^{-1} \int \log \tau(z) \rho(z) dz \right\}$.

Applying eqn (7) to the $\tau(z)$ profile for the 18 nm film at $T = 425\text{K}$, we obtain $\log \tau_{\text{film}} = -4.88$. At this temperature the predicted enhancement in the dynamics is $\Delta \log \tau = -1.4$ relative to the corresponding bulk ($\log \tau = -3.48$). As discussed above, an enhancement in the dynamics is expected because the presence of a free surface leads to an intermolecular environment characteristic of lowered density.

Based on a series of individual $\tau(z)$ profiles obtained over a range of incremented temperatures we used eqn (7) to calculate the overall relaxation times of the 18 nm freestanding P2ClS film (τ_{film}) as a function of T . These model predictions are shown in the $\log \tau$ vs. $1/T$ plot in Fig. 6 (red curve) together with the corresponding model curve for bulk (blue curve), as well as the experimental data for both the bulk (blue symbols) and the 18 nm film (red symbols). All results correspond to ambient pressure ($P = 1 \text{ atm}$). Also shown for reference are the data discussed above for the bulk-like 120 nm film from Fukao, et al.⁶⁵ (open red symbols).

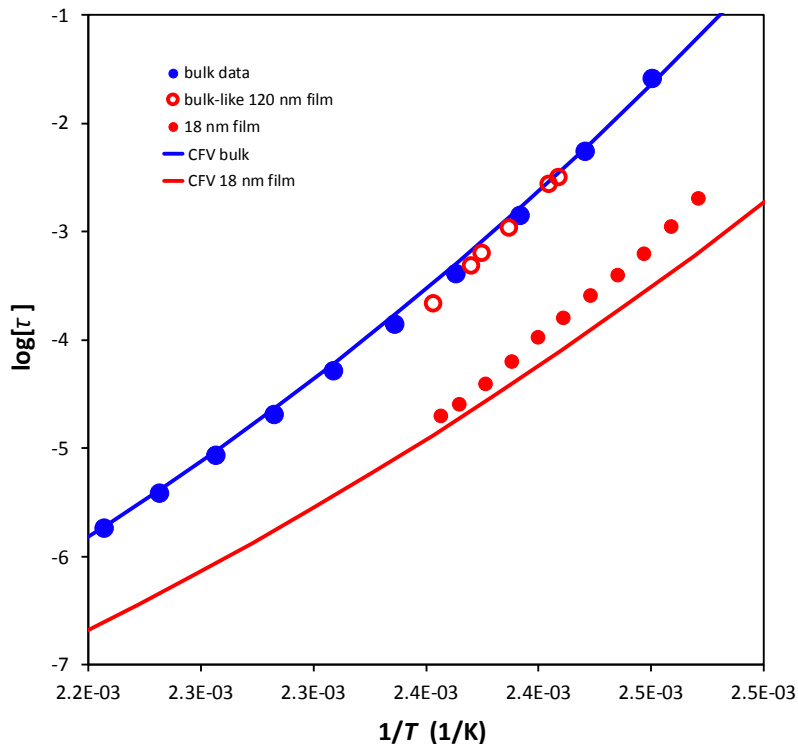


Fig. 6 Predicted relaxation times for the whole film sample as a function of inverse temperature. The CFV model prediction for the 18 nm freestanding P2CIS film is shown by the red curve with the corresponding model curve for the (ambient) bulk shown by the blue curve for comparison. The experimental data for bulk are from Schwartz et al.⁵³ and are shown by solid blue symbols; these data were used to parameterize the CFV model. The experimental data for the 18 nm film and the thicker 120 nm bulk-like film come from Fukao et al.⁶⁵ and are shown by solid red symbols and open red symbols respectively; see main text and the caption of Fig. 5 for more details on the data.

The model predictions for τ_{film} (Fig. 6) are in semi-quantitative agreement with the experimental P2CIS film data. *No data on the film was used to fit the model* and yet the shift in the dynamics relative to bulk is predicted within about 20%. As discussed above, the bulk $L_{\text{coop:ref}}$ value at $T_{\text{ref}} = 425\text{K}$ (used to fix v^* for the prediction of $L_{\text{coop}}(z)$) was set at 3.5 nm, ~ 2.3 Kuhn lengths; the over-prediction of the model with the approximated $L_{\text{coop:ref}} = 3.5$ nm indicates that a fitted $L_{\text{coop:ref}}$ value would turn out to be closer to about 3 nm.

As expected from the multiplicative coupling of temperature- and density-based contributions in eqn (1), both the model and the data (Fig. 6) clearly show that as T decreases ($1/T$ increases) there is an increasing sensitivity to confinement, i.e. the separation in τ between film and bulk is increasing. In this particular case, the model predicts a somewhat stronger growth in separation, however this might be partially explained by the inevitable small differences that arise between experiments and samples. Here, as noted above, we have the film data from Fukao et al.⁶⁵ and the bulk data from Schwartz et al.,⁵³ and it is the latter results to which the model was parameterized. For example, the model bulk curve, and thus the model film curve, would be slightly steeper if the model had been parameterized using the bulk-like 120 nm film data, instead.

5 Summary

In this work we predict the dynamic relaxation behavior of P2CIS freestanding films, and compared with experimental results. *We do not use any experimental film data in order to generate these predictions, only data on bulk samples.* The analysis succeeds because we were able to exploit our prior work showing that effects on dynamics induced by free interfaces are analogous to the effects induced by density (pressure) changes in the bulk. This meant that we could apply the CFV rate model to freestanding films using the results from LCL EOS analysis of the bulk behavior of P2CIS, along with the CFV characteristic parameters that describe bulk temperature and density dependent relaxation behavior.

An essential aspect of this process requires the CFV prediction of an *averaged local density profile* $\rho_{av}(z)$, which is key to explaining the experimental fact that relaxation profiles $\tau(z)$ are significantly broader than the sharp change in the position dependent (not averaged) density $\rho(z)$

of the sample within a few nm from the free surface. The path to the averaged density profile $\rho_{av}(z)$ involves translating the CFV model characteristic critical free volume, v^* , required for local segmental motion, into a temperature and density dependent cooperative lengthscale that represents the region around which free volume is gathered to enable relaxation.

Further, for the first time here, we use our predicted position dependent relaxation profile $\tau(z)$ to estimate a whole-sample-averaged characteristic relaxation time, in analogy to what is recorded experimentally. A key aspect of our analysis involves showing that the correct procedure is to average the $\ln \tau$ values at each position, not to average the bare τ values, themselves.

Here we summarize some of the specific key findings: Our initial analysis of the P2CIS bulk results demonstrated, again, the strong correlation between experimentally measured pressure dependent *dynamics* data and independently calculated free volume values from *thermodynamic PVT* data. In accordance with the CFV $\log \tau \sim f(T) \times (1/V_{free})$ prediction, P2CIS follows a pattern of linear $\log \tau$ vs. $1/V_{free}$ isotherms with T -dependent slopes.

In modeling the P2CIS free surface, the local density profile, $\rho(z)$, was calculated based on LCL EOS analysis of *PVT* and surface tension data. In addition to $\rho(z)$, we determined the cooperative length scale as a function of distance from the interface $L_{coop}(z)$; this defines the region relevant for collecting the critical free volume, v^* needed for local segmental relaxation. CFV predicts that $L_{coop}(z)$ decreases on moving toward the free surface because a smaller region will suffice as local free volume becomes more plentiful per segment. With both $L_{coop}(z)$ and $\rho(z)$ in hand, we were then able to predict the locally averaged position-dependent density profile, $\rho_{av}(z)$.

From $\rho_{av}(z)$, and thus $(V_{free}/V_{hc})(z)$, the CFV model (eqn (5)) was applied to predict relaxation times, $\tau(T,z)$, across the interface using the same characteristic parameters that had successfully described the bulk. Consistent with findings from simulations, the relaxation profiles were predicted to be broad, with the interfacial effect on dynamics extending several times deeper (~ 4 nm) into the bulk than does the much narrower local density profile, $\rho(z)$ (~ 1 nm).

The CFV $\tau(z)$ profile for the entire freestanding film was used to predict the film-averaged relaxation time, τ_{film} . We found that the decision about how to undertake the averaging is key. A simple mass weighted average, the mean, of $\tau(z)$ will overweight the largest relaxation times and cannot lead to sensible results. Instead, the mass weighted mean of $\log \tau(z)$ is the more logical choice, because it leads to an average that more closely corresponds to the most probable value (i.e. the peak) in the dielectric ϵ'' vs. $\log f$ relaxation spectrum.

The model predictions for τ_{film} as a function of temperature were compared with corresponding experimental results on stacked freestanding films and found to be in semi-quantitative agreement, within about 20%. The model predicts (and experimental data show) that at about 25 degrees above T_g , 18 nm freestanding P2CIS films have dynamics that are enhanced relative to bulk by about $\Delta \log \tau \approx -1.4$. In addition, consistent with the consequences of the fundamental $f(T) \times g(V)$ multiplicative coupling in eqn (1), both the model and experimental data show that the separation between relaxation times of bulk and film grows as T decreases ($f(T)$ increases).

In this paper we stretch the application of our Cooperative Free Volume model considerably, and show that the demanding goal of predicting dynamic relaxation in freestanding films can be achieved by a simple model, simply tethered to clear physics, implemented using data on bulk samples, alone.

Supplementary information

Electronic supplementary information (ESI) available: Details on LCL EOS analysis of *PVT* data to obtain P2CIS free volume values and P2CIS local density profiles.

Conflicts of interest

There are no conflicts to declare

Acknowledgments

We gratefully acknowledge the financial support provided by the National Science Foundation DMR-2006504.

References

- 1 C. Roland, S. Hensel-Bielowka, M. Paluch and R. Casalini, *Rep. Prog. Phys.*, 2005, **68**, 1405–1478.
- 2 G. Floudas, M. Paluch, A. Grzybowski and K. Ngai, *Molecular Dynamics of Glass-Forming Systems - Effects of Pressure*, Springer, Berlin, 2011.
- 3 C. M. Roland, *Macromolecules*, 2010, **43**, 7875–7890.
- 4 F. H. Stillinger and P. G. Debenedetti, *Annu. Rev. Condens. Matter Phys.*, 2013, **4**, 263–285.
- 5 C. Angell, K. Ngai, G. McKenna, P. McMillan and S. Martin, *J. Appl. Phys.*, 2000, **88**, 3113–3157.
- 6 G. B. McKenna and S. L. Simon, *Macromolecules*, 2017, **50**, 6333–6361.
- 7 L. Berthier and G. Biroli, *Rev. Mod. Phys.*, 2011, **83**, 587–645.
- 8 J. C. Dyre, *J. Phys. Chem. B*, 2014, **118**, 10007–10024.
- 9 D. Cangialosi, *J. Phys.-Condens. Matter*, 2014, **26**, 153101–153101.
- 10 S. Napolitano, E. Glynos and N. B. Tito, *Rep. Prog. Phys.*, 2017, **80**, 036602–036602.
- 11 M. D. Ediger and J. A. Forrest, *Macromolecules*, 2014, **47**, 471–478.
- 12 R. Richert, *Annu. Rev. Phys. Chem.*, 2011, **62**, 65–84.
- 13 M. Alcoutlabi and G. McKenna, *J. Phys.-Condens. Matter*, 2005, **17**, R461–R524.
- 14 D. S. Simmons, *Macromol. Chem. Phys.*, 2016, **217**, 137–148.
- 15 K. S. Schweizer and D. S. Simmons, *J. Chem. Phys.*, 2019, **151**, 240901.
- 16 J. Baschnagel and F. Varnik, *J. Phys.-Condens. Matter*, 2005, **17**, R851–R953.
- 17 D. Cangialosi, A. Alegria and J. Colmenero, *Prog. Polym. Sci.*, 2016, **54–55**, 128–147.
- 18 V. M. Boucher, D. Cangialosi, H. Yin, A. Schoenhals, A. Alegria and J. Colmenero, *Soft Matter*, 2012, **8**, 5119–5122.
- 19 K. Fukao and Y. Miyamoto, *Phys. Rev. E*, 2000, **61**, 1743–1754.
- 20 R. D. Priestley, D. Cangialosi and S. Napolitano, *J. Non-Cryst. Solids*, 2015, **407**, 288–295.
- 21 F. Kremer, M. Tress and E. U. Mapesa, *J. Non-Cryst. Solids*, 2015, **407**, 277–283.
- 22 R. P. White and J. E. G. Lipson, *Phys. Rev. Lett.*, 2020, **125**, 058002.
- 23 R. P. White and J. E. G. Lipson, *Macromolecules*, 2018, **51**, 7924–7941.
- 24 A. Debot, R. P. White, J. E. G. Lipson and S. Napolitano, *ACS Macro Lett.*, 2019, **8**, 41–45.
- 25 R. P. White and J. E. G. Lipson, *Macromolecules*, 2021, **54**, 4136–4144.

- 26K. Adrjanowicz, K. Kaminski, K. Koperwas and M. Paluch, *Phys. Rev. Lett.*, 2015, **115**, 265702–265702.
- 27M. Tarnacka, W. K. Kipnusu, E. Kaminska, S. Pawlus, K. Kaminski and M. Paluch, *Phys. Chem. Chem. Phys.*, 2016, **18**, 23709–23714.
- 28K. Adrjanowicz, K. Kaminski, M. Tarnacka, G. Szklarz and M. Paluch, *J. Phys. Chem. Lett.*, 2017, **8**, 696–702.
- 29K. Adrjanowicz, R. Winkler, A. Dzieńia, M. Paluch and S. Napolitano, *ACS Macro Lett.*, 2019, **8**, 304–309.
- 30W. K. Kipnusu, M. Elsayed, W. Kossack, S. Pawlus, K. Adrjanowicz, M. Tress, E. U. Mapesa, R. Krause-Rehberg, K. Kaminski and F. Kremer, *J. Phys. Chem. Lett.*, 2015, **6**, 3708–3712.
- 31W. K. Kipnusu, M. M. Elmandy, M. Elsayed, R. Krause-Rehberg and F. Kremer, *Macromolecules*, 2019, **52**, 1864–1873.
- 32M. Tarnacka, M. Mierzwa, E. Kaminska, K. Kaminski and M. Paluch, *Nanoscale*, 2020, **12**, 10600–10608.
- 33R. P. White and J. E. G. Lipson, *J. Chem. Phys.*, 2017, **147**, 184503–184503.
- 34R. P. White and J. E. G. Lipson, *Eur. Phys. J. E*, 2019, **42**, 100.
- 35R. P. White and J. E. G. Lipson, *Macromolecules*, 2016, **49**, 3987–4007.
- 36J. E. G. Lipson and R. P. White, *J. Chem. Eng. Data*, 2014, **59**, 3289–3300.
- 37D. Long and F. Lequeux, *Eur. Phys. J. E*, 2001, **4**, 371–387.
- 38S. Merabia, P. Sotta and D. Long, *Eur. Phys. J. E*, 2004, **15**, 189–210.
- 39T. Salez, J. Salez, K. Dalnoki-Veress, E. Raphael and J. A. Forrest, *Proc. Natl. Acad. Sci. U. S. A.*, 2015, **112**, 8227–8231.
- 40A. D. Phan and K. S. Schweizer, *Macromolecules*, 2018, **51**, 6063–6075.
- 41J. E. G. Lipson and S. T. Milner, *Eur. Phys. J. B*, 2009, **72**, 133–137.
- 42R. Casalini, U. Mohanty and C. M. Roland, *J. Chem. Phys.*, 2006, **125**, 014505–014505.
- 43R. Casalini and C. M. Roland, *J. Non-Cryst. Solids*, 2007, **353**, 3936–3939.
- 44N. Gnan, T. B. Schroder, U. R. Pedersen, N. P. Bailey and J. C. Dyre, *J. Chem. Phys.*, 2009, **131**, 234504.
- 45A. Grzybowski and M. Paluch, in *The Scaling of Relaxation Processes*, eds. F. Kremer and A. Loidl, Springer International Publishing, Cham, 2018, pp. 77–119.
- 46D. Diaz-Vela, J.-H. Hung and D. S. Simmons, *ACS Macro Lett*, 2018, **7**, 1295–1301.

- 47R. P. White and J. E. G. Lipson, *J. Phys. Chem. B*, 2021, **125**, 4221–4231.
- 48C. M. Roland, K. J. McGrath and R. Casalini, *Macromolecules*, 2006, **39**, 3581–3587.
- 49G. Adam and J. H. Gibbs, *J. Chem. Phys.*, 1965, **43**, 139–146.
- 50R. P. White and J. E. G. Lipson, *Rubber Chem. Technol.*, 2019, **92**, 612–624.
- 51R. P. White and J. E. G. Lipson, *Acs Macro Lett.*, 2017, **6**, 529–534.
- 52R. P. White and J. E. G. Lipson, *Macromolecules*, 2018, **51**, 4896–4909.
- 53G. A. Schwartz, J. Colmenero and A. Alegria, *Macromolecules*, 2006, **39**, 3931–3938.
- 54I. C. Sanchez, *Physics of Polymer Surfaces and Interfaces*, Butterworth, Greenwich, CT, 1992.
- 55C. I. Poser and I. C. Sanchez, *J. Colloid Interface Sci.*, 1979, **69**, 539–548.
- 56G. Dee and B. Sauer, *Adv. Phys.*, 1998, **47**, 161–205.
- 57S. Wu, *J. Phys. Chem.*, 1970, **74**, 632-.
- 58L. Lee, *J. Appl. Polym. Sci.*, 1968, **12**, 719–730.
- 59P. Z. Hanakata, J. F. Douglas and F. W. Starr, *J. Chem. Phys.*, 2012, **137**, 244901.
- 60P. Z. Hanakata, B. A. P. Betancourt, J. F. Douglas and F. W. Starr, *J. Chem. Phys.*, 2015, **142**, 234907–234907.
- 61D. M. Sussman, S. S. Schoenholz, E. D. Cubuk and A. J. Liu, *Proc. Natl. Acad. Sci. U. S. A.*, 2017, **114**, 10601–10605.
- 62A. Shavit and R. A. Riggleman, *Macromolecules*, 2013, **46**, 5044–5052.
- 63A. Shavit and R. A. Riggleman, *J. Phys. Chem. B*, 2014, **118**, 9096–9103.
- 64T. P. Lodge and T. C. B. McLeish, *Macromolecules*, 2000, **33**, 5278–5284.
- 65K. Fukao, T. Terasawa, Y. Oda, K. Nakamura and D. Tahara, *Phys. Rev. E*, 2011, **84**, 041808.
- 66R. J. Lang and D. S. Simmons, *Macromolecules*, 2013, **46**, 9818–9825.
- 67Y. P. Koh and S. L. Simon, *J. Polym. Sci. Part B-Polym. Phys.*, 2008, **46**, 2741–2753.
- 68Y. P. Koh, G. B. McKenna and S. L. Simon, *J. Polym. Sci. Part B-Polym. Phys.*, 2006, **44**, 3518–3527.
- 69A. Schonhals and F. Kremer, *Broadband Dielectric Spectroscopy*, Springer, Berlin, 2003.